Structural Characterization and Study of Adsorbate Interactions with Cu(II) Ions in SBA-15 Materials by Electron Spin Resonance and Electron Spin−Echo Modulation Spectroscopies

Ayaluru Murali, Zhixiang Chang, Koodali T. Ranjit, Ravoori Murali Krishna, Vadim Kurshev, and Larry Kevan*

Department of Chemistry, University of Houston, Houston, Texas 77204-5003

Received: November 27, 2001; In Final Form: March 19, 2002

Mesoporous SBA-15 materials have been synthesized with different pore sizes and characterized by X-ray diffraction, N_2 adsorption isotherms, X-ray fluorescence and thermal gravimetric analysis. SBA-15 has been aluminated by grafting $AlCl_3$ to SBA-15 in the presence of ethanol. Cupric ions have been introduced into these materials by aqueous ion-exchange. The electron spin resonance (ESR) spectrum of as-synthesized Cu−AlSBA-15 materials shows an axial *g* factor for Cu(II), and the *g* and hyperfine parameters show that the cupric ions have octahedral or square pyramidal symmetry. ESR and electron spin−echo modulation spectra have been analyzed to determine the coordination geometry of adsorbates including CH_3OD, D_2O, ND_3, $^{15}NH_3$, and C_2D_4 to cupric ions.

Introduction

Porous oxide materials find a wide variety of industrial applications as ion-exchangers, sorbents, and catalysts.[1] Porous materials are divided into three categories—microporous, mesoporous, and macroporous materials—depending on their pore sizes. Microporous materials, typically zeolites and aluminophosphates, contain pores with diameters up to 20 Å, while mesoporous materials have pores with diameters in the range 20−500 Å. Porous materials with pore diameters >500 Å are termed macroporous materials. Recently, much attention has been given to the synthesis and characterization of mesoporous materials. Among the mesoporous materials so far reported, the most popular ones are the M41S family of materials reported by Mobil,[2] MSU materials reported by Pinnavaia and co-workers[3] from Michigan State University and SBA materials reported by Stucky and co-workers[4,5] from the University of California at Santa Barbara. The M41S materials have pores from 15 to 100 Å ordered in hexagonal (MCM-41), cubic (MCM-48), and laminar (MCM-50) arrays with a typical wall thickness of about 10 Å. Synthesis of M41S materials involves use of cationic surfactants,[2] while SBA-15 and MSU materials are prepared from nonionic surfactants.[3−5]

SBA-15, with pore sizes up to 300 Å, is a promising material for catalysis of large molecules. It has a hexagonal structure with well-resolved powder X-ray diffraction (XRD) peaks and a large unit cell parameter. It is interesting to note that these materials have high thermal stability because of their thick pore walls (≈60 Å). It retains its hexagonal structure even after heating to 1123 K.[5] Also, its pore size can be varied from 89 to 300 Å by changing the ratio of surfactant triblock glycol copolymer to cosolvent trimethylbenzene.[4] Recently, applications of SBA-15 type materials to waveguides,[6] fibers,[7] mesocellular foams,[8] and protein sequesterization and release[9] have been reported.

Pure siliceous SiSBA-15 ideally has no acid sites, although in practice a few acid sites are present associated with residual hydroxyl groups. The introduction of framework aluminum into tetrahedral framework sites of SBA-15 forms both acid and ion-exchange sites. The process of alumination can be done in two ways. The aluminum precursor can be added to the gel during direct synthesis or it can be grafted onto the walls of SiSBA-15 by postsynthesis methods. Since SBA-15 materials are prepared under highly acidic conditions in which most of the aluminum salts dissolve, alumination can only be done using such postsynthesis techniques. Luan et al.[10] studied the alumination of SBA-15 materials by three postsyntheses. Yue et al.[11] reported the direct synthesis of AlSBA-15. The present work deals with AlSBA-15 prepared by a postsynthesis method.

Luan et al.[10] studied the ion-exchange capacity of AlSBA-15 with copper as a transition metal ion probe. They synthesized AlSBA-15 with different Si/Al ratios and also explored different aluminum sources for alumination. It was shown that the surface area and pore volume are strong functions of the Si/Al ratio and the aluminum source. It was also shown that AlSBA-15 with $AlCl_3$ as the aluminum source and a Si/Al ratio of 10 gives the maximum ion-exchange capacity.

The present work aims at further investigation of Cu−AlSBA-15 materials. SBA-15 materials with different pore sizes have been synthesized and characterized using X-ray fluorescence (XRF), X-ray diffraction (XRD), thermogravimetric analysis (TGA), and N_2 adsorption isotherms. These materials were aluminated and then ion-exchanged with $CuSO_4$ solution. Adsorbate geometries with the cupric ions were determined by interacting these materials with different deuterated and ^{15}N labeled adsorbates and measuring weak dipolar interactions between the cupric ions and magnetic nuclei in the adsorbate by electron spin resonance (ESR) and electron spin−echo modulation (ESEM) spectroscopies.

ESR and ESEM are proven techniques to locate copper ion sites and determine their adsorbate geometries in both microporous and mesoporous oxide materials.[12−15] ESR gives information regarding the site symmetry around the Cu(II) ions while ESEM analysis gives information regarding the number and distance of magnetic nuclei in adsorbates coordinating to Cu(II) ions.

10.1021/jp014325t CCC: $22.00
Published on Web 06/14/2002

Experimental Section

Synthesis. The synthesis of SBA-15 has been carried out as reported.[4,5] In the present work, 3.2 g of amphiphilic triblock copolymer, poly(ethylene glycol)-*block*-poly(propylene glycol)-*block*-poly(ethylene glycol) (average molecular weight 5800, Aldrich) was dispersed in 24 g of water and 96 g of 2 M HCl with stirring. Once the triblock copolymer was completely dissolved, 6.8 g of tetraethyl orthosilicate (TEOS, Aldrich) was added to the above homogeneous solution with stirring. The gel was stirred at 40 °C for 24 h and then crystallized in a Teflon bottle at 100 °C for 48 h. After crystallization, the solid product was filtered, washed with deionized water, and dried in air at room temperature. The material was calcined in static air at 550 °C for 12 h to decompose the triblock copolymer and to obtain a white powder (SBA-15).

The synthesis of SBA-15 with larger pore sizes is similar except for the addition of a cosolvent, 1,3,5-trimethylbenzene (TMB), and a lower crystallization temperature. Different amounts of TMB were added to a homogeneous solution of triblock copolymer, water, and 2 M HCl, the resulting solution was stirred for 1 h, and then TEOS was added. After the resulting gel was stirred at 40 °C for 24 h, the gel was allowed to crystallize at 80 °C for 48 h. The resulting materials were filtered, washed with deionized water, and dried in air at room temperature. The material was then calcined in static air at 550 °C for 12 h. These materials are denoted as SBA-15-(*D* Å), where *D* represents the pore diameter of the material measured from adsorption isotherms.

The alumination of SBA-15 was done in the following manner. Silica SBA-15 was combined with 50 mL of dry ethanol in a N_2 atmosphere containing various amounts of $AlCl_3$ and stirred at room temperature for 12 h. The resulting solid material was then filtered, washed vigorously with dry ethanol, and dried in air at room temperature. Then the solid powder was calcined at 550 °C for 5 h. The resulting material is designated as AlSBA-15-(*D* Å)-(*X*), where *X* is the Si/Al ratio from the chemical stoichiometric composition in the postsynthesis mixtures. These materials were then ion-exchanged by stirring a powder sample of AlSBA-15-(*D* Å)-(*X*) in a 20 times by weight solution of 1 N $CuSO_4$ for 5 h at 50 °C. The resultant solid was then filtered out and washed with hot distilled water to remove any physically adhered Cu(II) ions. The resulting material is designated as Cu−AlSBA-15-(*D* Å)-(*X*).

Characterization. The elemental compositions of the materials reported in the present work were analyzed by a Kevex X-ray fluorescence spectrometer using a Ti secondary target and operating at 25 kV and 2.5 mA. The elemental composition was computed by comparing the spectra with standards of known concentration.

Low angle powder XRD patterns were collected at room temperature before and after calcination using a Scintag XDS 2000 automated diffractometer with Cu Kα radiation and equipped with a liquid nitrogen cooled germanium solid-state detector.

N_2 adsorption isotherms were measured at 77 K using a Micrometrics Gemini 2375 analyzer. The volume of adsorbed N_2 was normalized to standard temperature and pressure. Prior to experiments, samples were dehydrated at 250 °C for 5 h to remove adsorbed water. The specific surface area, A_{BET}, was determined from the linear part of the BET equation ($P/P_0 = 0.05-0.30$). The calculation of mesopore size distribution was performed using the adsorption branches of N_2 adsorption isotherms and the Barrett−Joyner−Halenda (BJH) formula.[16] The mesopore surface area, A_{BJH}, volume, V_{BJH}, and pore diameter, D_{BJH}, were obtained from the pore size distribution curves.

Thermal analysis of the samples were carried out on a TA Instruments TGA 2050 thermal analyzer with a heating rate of 10 K min^{-1} in the presence of oxygen flow.

ESR and ESEM Measurements. Cu−AlSBA-15-(*D* Å)-(*X*) samples were loaded directly into a Suprasil quartz ESR tube (2 mm i.d. by 3 mm o.d.), which could be connected to a vacuum and gas handling line. Dehydration of the sample was carried out by first evacuating the tube at room temperature followed by heating to 400 °C over a period of ∼10 h. Following this evacuation, the sample was exposed to 50 kPa of static high purity dry oxygen for 10 h at 400 °C in order to reoxidize any copper species that was reduced during the heating period. Finally, the oxygen was evacuated at room temperature to a pressure of 10^{-5} kPa. This heat-treated sample with oxygen is termed as a dehydrated sample.

After dehydration, adsorbates were admitted at room temperature to the sample tubes and left to equilibrate. Deuterated adsorbates CH_3OD and D_2O were obtained from Aldrich, while ND_3, C_2D_4, and $^{15}NH_3$ were obtained from Cambridge Isotope Laboratories and used after repeated freeze−pump−thaw cycles.

ESR spectra were recorded at room temperature and at 77 K on an ESP 300 Bruker ESR spectrometer. ESEM measurements were performed on an ESP 380 Bruker FT ESR spectrometer at 4 K using the three pulse echo sequence, $\pi/2-\tau-\pi/2-T-\pi/2-$echo.[17] The deuterium nuclear modulation pattern was simulated and fitted to the experimental data by a least squares procedure.[18] The parameters are the number of interacting nuclei *N*, their distance *R* from the paramagnetic center, and their isotropic hyperfine interaction A_{iso}. For a deuterated or partially deuterated adsorbate, simulation of the deuterium modulation in terms of the number and distance of the nearest neighbor deuterium nuclei to Cu(II) gives the number and distance of adsorbate molecules interacting with Cu(II). If the distance corresponds to a direct coordination distance, a strong interaction with the adsorbate is indicated. When the distance is significantly greater than direct coordination, only a weak interaction with the adsorbate is indicated. This method has been well discussed.[17,18]

Results

Characterization. Figure 1 shows the X-ray diffraction patterns for SBA-15-(90 Å) before and after calcination. The patterns resemble the one reported for hexagonal SBA-15 materials.[4,10] As can be observed from Figure 1, the uncalcined sample exhibits one strong peak corresponding to the 100 reflection ($d = 114.6$ Å) and two weak and less well resolved peaks corresponding to reflections from the 110 and 200 planes. Upon calcination, the sample shows five well-resolved peaks in its X-ray diffraction pattern. These peaks are assigned to the reflections from the 100, 110, 200, 210, and 300 planes in increasing order of 2θ. From Figure 1, it is quite evident that the peak intensity and the resolution improves after calcination. It is interesting to note that the peak positions are not shifted after calcination, whereas a shift toward higher reflection angles for calcined samples was reported for SBA-15 previously.[4] A shift toward higher angles indicates a slight contraction of the pores. Since, there is no shift in the peak positions after calcination in our materials, it is evident that the hexagonal structure is stable and perhaps improves its order after calcination, as seen by the more intense and better resolved peaks. Luan et al.[10] also reported similar results for SBA-15 where the peak positions are not shifted after calcination.

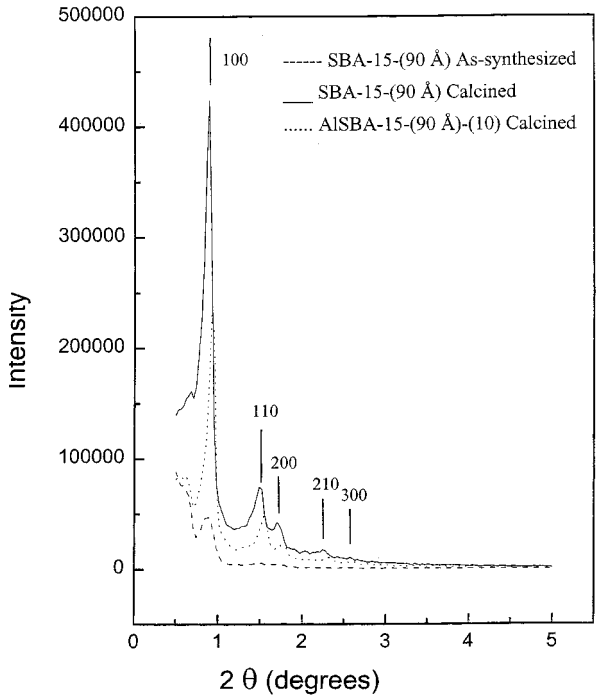

Figure 1. Low angle X-ray diffraction patterns for SBA-15-(90 Å) before calcination (- - -), after calcination (—), and for calcined AlSBA-15-(90 Å)-(Si/Al). The *hkl* values are marked for calcined SBA-15-(90 Å).

The X-ray diffraction patterns for AlSBA-15-(90 Å) were also collected (see Figure 1). Interestingly, a shift toward higher 2θ values was observed as compared to the peak positions of calcined (as well as uncalcined) purely siliceous SBA-15 material. This indicates either a considerable contraction of the pores or a decrease in the thickness of the pore walls.[19]

SBA-15 materials with larger pore sizes (160 and 230 Å) were also prepared. The XRD spectra of those materials show a strong peak from the 100 plane and two weaker peaks corresponding to reflections from the 110 and 200 planes.

For all the samples, the unit cell parameter a_0 has been determined from the d value of the 200 reflection rather than from that of the 100 reflection using the formula $a_0 = 4d_{200}/\sqrt{3}$.[20] In all the samples, the 100 reflection occurred at very low angles of 2θ (typically less than 0.9°) and the instrumental uncertainty at that angle is greater than at the 200 reflection. Hence the lattice spacing between 200 reflections were taken to evaluate the unit cell parameter a_0.

The elemental analyses of all the samples were performed to monitor the alumination process and the ion-exchange capacity. Hence, attention has been given to the Si/Al ratio for all samples and also to the Cu/Si ratio for samples containing cupric ions. Table 1 gives the results of elemental analysis as calculated from XRF spectra of the various samples.

TGA spectra of some of the samples were recorded (spectra not shown) to compare the thermal behavior of the SBA-15 materials synthesized in the present work with those reported previously.[5] A clear weight loss of ≈35 wt % near 150 °C is observed, which is comparable to a 46 wt % weight loss at 145 °C reported by Zhao et al.[5] The TGA spectrum of SBA-15-(230 Å) (not shown) also shows similar behavior with a weight loss of 53 wt % near 150 °C. After calcination, no TGA peaks are seen, which indicates that the triblock copolymer has been removed during calcination.

N_2 adsorption isotherms were recorded for all the SBA-15 materials to determine the pore size parameters. Figure 2 shows

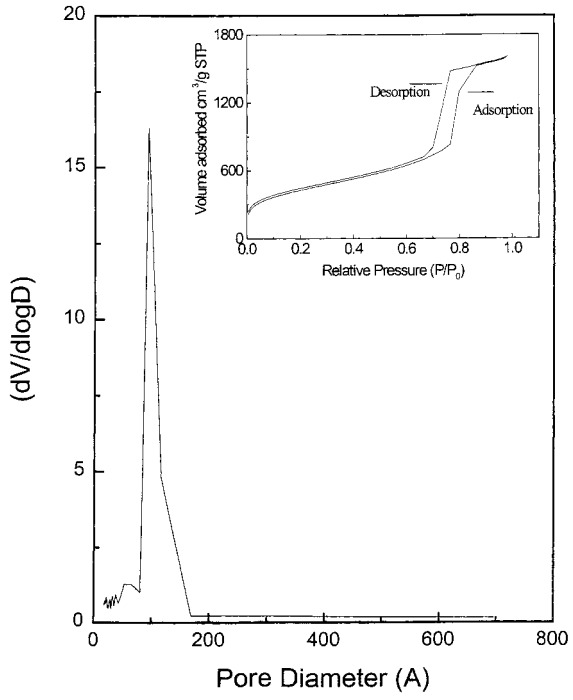

Figure 2. N_2 adsorption isotherm (inset) and pore size distribution curve for SBA-15-(90 Å).

TABLE 1: Results of Elemental Analyses of Various SBA-15-(Pore Size)-(Si/Al) Materials

sample	Si/Al	Cu/Si
AlSBA-15-(90 Å)−(10)	9.2	
AlSBA-15-(90 Å)−(40)	27	
AlSBA-15-(170 Å)−(10)	14	
Cu−AlSBA-15-(90 Å)−(10)	13	0.20
Cu−AlSBA-15-(90 Å)−(40)	23	0.09
Cu−AlSBA-15-(170 Å)−(10)	5.1	0.18

TABLE 2: Pore Size Distribution Parameters for Various SBA-15-(Pore Size) Materials

sample	A_{BET} ($m^2\ g^{-1}$)	$A_{Langmuir}$ ($m^2\ g^{-1}$)	D (Å)	A_{BJH} ($m^2\ g^{-1}$)	V_{BJH} ($cm^3\ g^{-1}$)
SBA-15-(90 Å)	612	970	90	554	1.03
SBA-15-(170 Å)	837	1271	170	551	1.06
SBA-15-(230 Å)	1431	2183	230	979	2.38

the N_2 adsorption isotherm for SBA-15-(90 Å) and the pore size distribution. The N_2 adsorption isotherms for other samples are similar and not shown. Figure 2 shows an irreversible Type IV[21] adsorption isotherm. The pore size distribution was calculated using the BJH equation and shows a narrow pore size distribution with an average pore size of 90 Å. Table 2 lists pore size parameters for the other samples.

ESR and ESEM Studies. Figure 3 shows the ESR spectra of Cu−AlSBA-15-(90 Å)-(10) at room temperature as well as at 77 K. The room-temperature ESR spectrum shows two copper species. Species A has an anisotropic spectrum with $g_{||}^{A} = 2.369$, $A_{||}^{A} = 131 \times 10^{-4}\ cm^{-1}$, $g_{\perp}^{A} = 2.078$, and $A_{\perp}$ unresolved. Species A′ has an isotropic signal with $g_{iso}^{A'} = 2.154$. After cooling the sample to 77 K, a new copper species B develops with $g_{||}^{B} = 2.391$, $A_{||}^{B} = 146 \times 10^{-4}\ cm^{-1}$, $g_{\perp}^{B} = 2.068$, and $A_{\perp}^{B}$ unresolved.

ESR spectra of Cu(II) at room temperature (RT) and 77 K were simulated using the following axial spin Hamiltonian where the symbols have their usual meanings.

$$\mathcal{H} = \beta g_{||} H_z S_z + \beta g_{\perp}(H_x S_x + H_y S_y) + A_{||} S_z I_z + A_{\perp}(S_x I_x + S_y I_y)$$

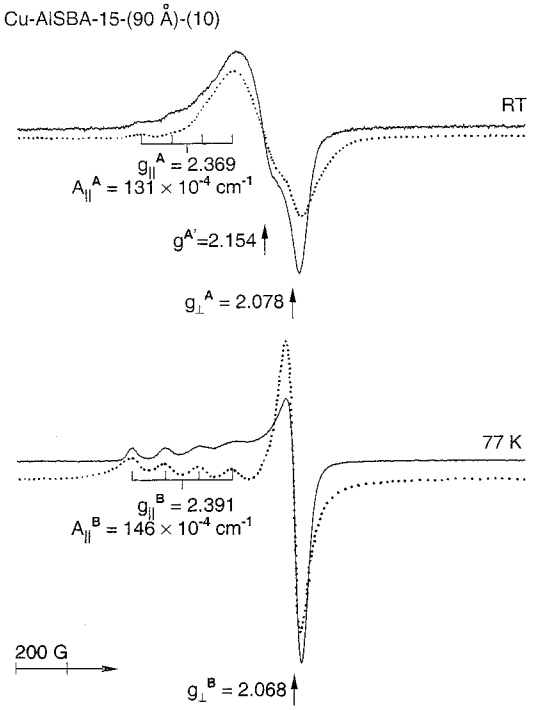

Figure 3. ESR spectra of Cu−AlSBA-15-(90 Å)-(10) at (a) room temperature (RT) and (b) 77 K. The dotted lines show corresponding simulated spectra; see text for parameters.

The WIN EPR SimFonia software version 1.25 of Bruker Instruments (1996) was used to simulate ESR spectra. The simulated spectra are shown as dotted lines in Figure 3 as representative examples. The parameters used for the RT simulation are $A_{\|} = 131 \times 10^{-4}$ cm^{-1}, $g_{\|} = 2.369$ (line width, $\Delta H = 80$ G, ratio of Lorentzian to Gaussian line shapes, L/G = 0.5), and $g_{\perp} = 2.08$ ($\Delta H = 70$ G, L/G = 1.0) superimposed on an isotropic signal with $g = 2.54$ ($\Delta H = 240$ G, L/G = 1.0). The parameters used for the 77 K simulation are $A_{\|} = 145 \times 10^{-4}$ cm^{-1}, $g_{\|} = 2.390$, ($\Delta H = 80$ G, L/G = 0 or purely Gaussian), and $g_{\perp} = 2.08$ ($\Delta H = 60$ G, L/G = 0).

A new copper species C with g and A parameters of $g_{\|}^{C} = 2.353$, $A_{\|}^{C} = 143 \times 10^{-4}$ cm^{-1}, $g_{\perp}^{C} = 2.096$, and $A_{\perp}^{C}$ unresolved, evolves after evacuation for 2 h at room temperature. Figure 4 shows the ESR spectra of Cu−AlSBA-15-(90 Å)-(10) after evacuation at room temperature for different times. In Figure 4 isotropic species A′ decreases after 2 h evacuation and completely disappears after 4 h evacuation, forming another species D with g and A parameters of $g_{\|}^{D} = 2.343$, $A_{\|}^{D} = 152 \times 10^{-4}$ cm^{-1}, $g_{\perp}^{D} = 2.065$, and $A_{\perp}^{D}$ unresolved. The ESR spectra of Cu−AlSBA-15-(90 Å)-(10) after evacuation at different temperatures together with the ESR spectrum of dehydrated Cu−AlSBA-15-(90 Å)-(10) are shown in Figure 5. The ESR spectrum of Cu−AlSBA-15-(90 Å)-(10) evacuated for 2 h at 100 °C shows parameters $g_{\|} = 2.353$, $g_{\perp} = 2.088$, $A_{\|} = 143 \times 10^{-4}$ cm^{-1}, and $A_{\perp}$ unresolved. These parameters are similar to those of species C. After the sample is heated to 400 °C and evacuated for 10 h, a new species E results with $g_{\|}^{E} = 2.316$, $A_{\|}^{E} = 163 \times 10^{-4}$ cm^{-1}, $g_{\perp}^{E} = 2.042$, and $A_{\perp}^{E} = 39 \times 10^{-4}$ cm^{-1}. Oxygen was allowed to interact with this sample at 400 °C for 10 h to reoxidize copper ions and then the sample was brought to room temperature over a period of 2 h and the oxygen was evacuated. This sample is termed a dehydrated sample and its ESR spectrum is shown in Figure 5c. This spectrum has parameters $g_{\|} = 2.348$, $g_{\perp} = 2.057$, $A_{\|} = 156 \times 10^{-4}$ cm^{-1}, and $A_{\perp}$ unresolved, which are similar to those of species D.

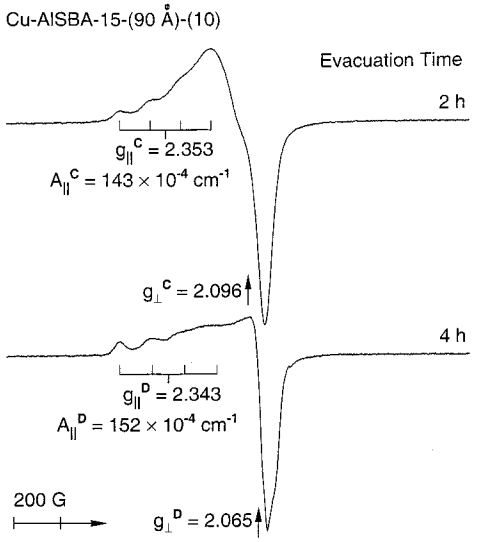

Figure 4. ESR spectra of Cu−AlSBA-15-(90 Å)-(10) at 77 K after evacuation at room temperature for (a) 2 h and (b) 4 h.

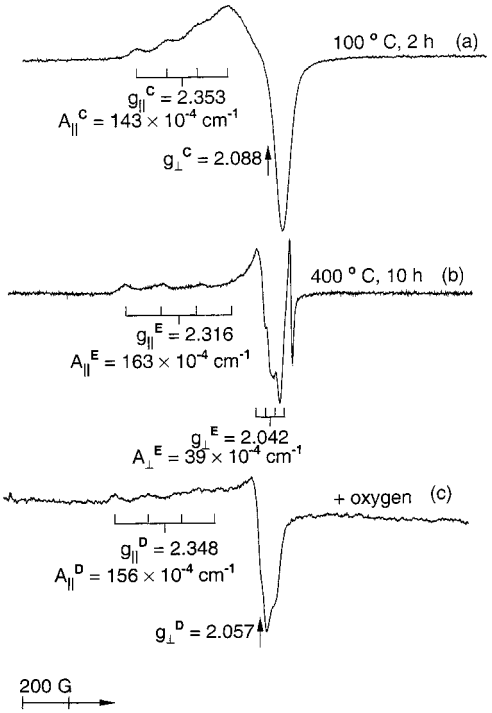

Figure 5. ESR spectra of Cu−AlSBA-15-(90 Å)-(10) at 77 K after evacuation at (a) 100 °C for 2 h, (b) 400 °C for 10 h, and (c) subsequent exposure to oxygen.

ESR spectra of Cu−AlSBA-15-(230 Å)-(Si/Al) were recorded at 77 K with Si/Al = 10, 20, and 40. Figure 6 shows the ESR spectrum of Cu−AlSBA-15-(230 Å)-(Si/Al) at 77 K with Si/Al = 40. No significant change in the g and A parameters with Si/Al ratio is observed. Thus, we can infer that the crystal field around cupric ions is not influenced by the Al nucleus. However, the doubly integrated intensity of the signal decreases with increasing Si/Al ratio. This indicates that the number of ion-exchange sites increases with a decrease in the Si/Al ratio. This is consistent with the analytical results in Table 1.

ESR spectra at 77 K of Cu−AlSBA-15-(90 Å)-(10) with different adsorbates including CH_3OD, D_2O, ND_3, C_2D_4, and $^{15}NH_3$ are shown in Figures 7−9. ESR spectra of Cu−AlSBA-15-(170 Å)-(10) and Cu−AlSBA-15-(230 Å)-(10) with the above adsorbates show the g and A parameters listed in Table 3.

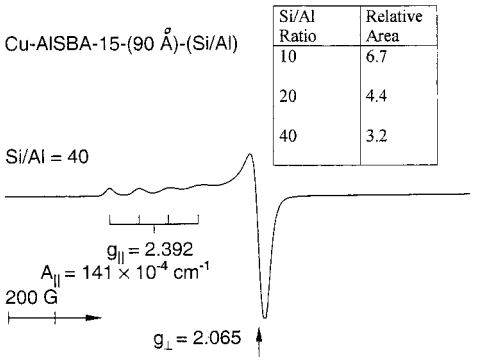

Si/Al Ratio	Relative Area
10	6.7
20	4.4
40	3.2

Figure 6. ESR spectra of Cu−AlSBA-15-(90 Å)-(Si/Al) at 77 K with Si/Al = 40. The relative areas for Si/Al = 10, 20, and 40 as obtained by double integration are also shown.

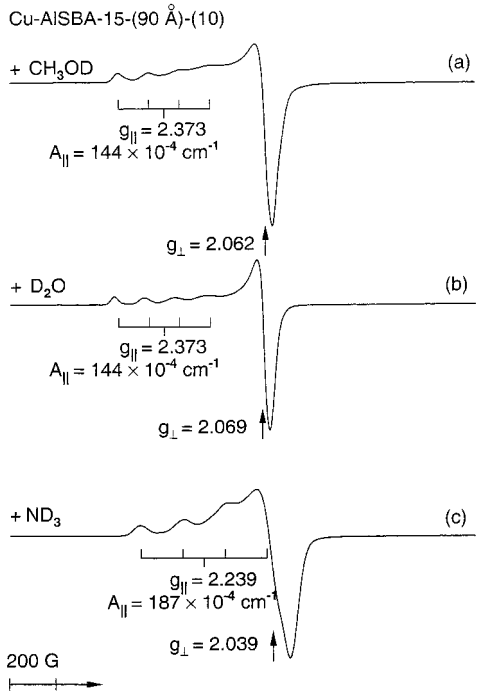

Figure 7. ESR spectra of Cu−AlSBA-15-(90 Å)-(10) at 77 K with adsorbed (a) CH_3OD, (b) D_2O, and (c) ND_3.

The ESR spectrum at 77 K of Cu−AlSBA-15-(90 Å)-(10) with adsorbed CH_3OD shown in Figure 7a has parameters $g_{||} = 2.373$, $g_{\perp} = 2.062$, $A_{||} = 144 \times 10^{-4}$ cm^{-1}, and $A_{\perp}$ unresolved. The ESR spectrum of Cu−AlSBA-15-(90 Å)-(10) with adsorbed D_2O in Figure 7b is similar to that with adsorbed CH_3OD.

Cu−AlSBA-15-(90 Å)-(10) with adsorbed ND_3 shows an ESR spectrum (Figure 7c) with $g_{||} = 2.239$, $g_{\perp} = 2.039$, $A_{||} = 187 \times 10^{-4}$ cm^{-1}, and $A_{\perp}$ unresolved, which are different from the parameters for other adsorbates. The ESR spectrum of Cu−AlSBA-15-(90 Å)-(10) with adsorbed $^{15}NH_3$ is similar (Figure 8), with comparable parameters except for an additional five line superhyperfine structure in the perpendicular part (Figures 8 b and c). It is observed that the color of the sample turns blue after adsorption of ammonia.

A new copper species is observed in Cu−AlSBA-15-(90 Å)-(10) with adsorbed C_2D_4 with $g_{||} = 2.329$, $g\perp = 2.038$, $A_{||} = 182 \times 10^{-4}$ cm^{-1}, and $A_{\perp} = 27 \times 10^{-4}$ cm^{-1} (Figure 9). Unlike the other adsorbates, C_2D_4 also shows a better resolved hyperfine structure in the $g_{\perp}$ region. A similar spectrum has been reported for Cu(II) ions in siliceous MCM-41.[22]

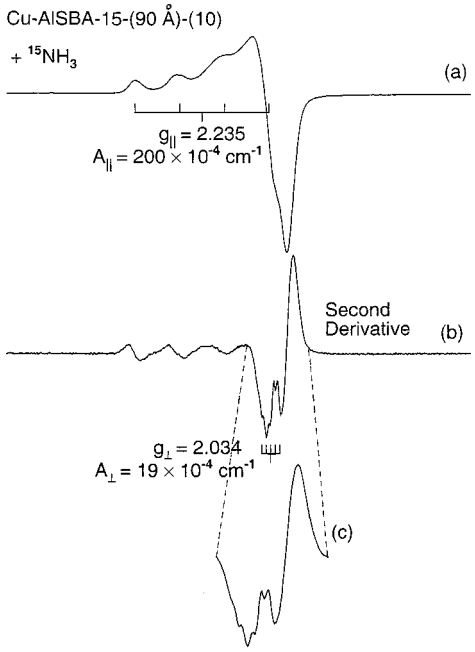

Figure 8. (a) ESR spectra of Cu−AlSBA-15-(90 Å)-(10) at 77 K with adsorbed $^{15}NH_3$, (b) second derivative of (a), and (c) expansion of the perpendicular part of (b).

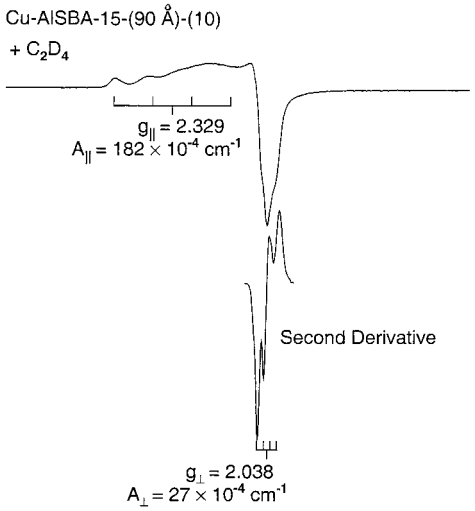

Figure 9. ESR spectra of Cu−AlSBA-15-(90 Å)-(10) at 77 K with adsorbed C_2D_4.

Table 3 shows the ESR parameters for different adsorbates versus pore size. There does not seem to be any consistent monotonic trend with pore size for the various adsorbates. For example, for C_2D_4 adsorbate $g_{||}$ increases for 90−170 Å pores and remains the same for 230 Å pores. In contrast, for CH_3OD adsorbate, $g_{||}$ is about constant for 90−170 Å pores and then decreases slightly for 230 Å pores. $A_{||}$ also shows different variations with pore size for different adsorbates.

Experimental and simulated ESEM spectra of Cu−AlSBA-15-(90 Å)-(10) with CH_3OD, D_2O, ND_3, and C_2D_4 adsorbates are shown in Figures 10 and 11. The simulation parameters for these spectra together with ones for Cu−AlSBA-15-(170 Å)-(10) and Cu−AlSBA-15-(230 Å)-(10) are listed in Table 4.

Discussion

Characterization. The unit cell parameter a_0 for SBA-15-(90 Å) calculated from the lattice spacing for the 200 reflection ($2\theta = 1.7°$) is 120 Å. This lattice spacing includes the pore

TABLE 3: Spin-Hamiltonian Parameters of Cu−AlSBA-15-(*D* Å)-(Si/Al) with Different Pore Sizes and Different Adsorbates

adsorbate	$g_{\|}$ [a]	$g_{\perp}$ [b]	$A_{\|}$ [b] ($\times 10^{-4}$ cm^{-1})	$A_{\perp}$ [c] ($\times 10^{-4}$ cm^{-1})
		Cu−AlSBA-15-(90 Å)-(10)		
CH_3OD	2.373	2.062	144	
D_2O	2.373	2.069	144	
ND_3	2.239	2.039	187	
$^{15}NH_3$	2.235	2.034	200	19[d]
C_2D_4	2.329	2.038	182	27
		Cu−AlSBA-15-(170 Å)-(10)		
CH_3OD	2.378	2.069	158	
D_2O	2.394	2.069	146	
ND_3	2.239	2.045	187	
$^{15}NH_3$	2.253	2.033	176	21[d]
C_2D_4	2.368	2.047	158	23
		Cu−AlSBA-15-(230 Å)-(10)		
CH_3OD	2.363	2.065	144	
D_2O	2.358	2.062	157	
ND_3	2.221	2.009	186	
$^{15}NH_3$	2.251	2.041	201	17[d]
C_2D_4	2.368	2.034	131	31

[a] Estimated errors in g values are $\pm$ 0.003. [b] Estimated error is $\pm 4 \times 10^{-4}$ cm^{-1}. [c] Estimated error is $\pm 2 \times 10^{-4}$ cm^{-1}. [d] ^{15}N superfine coupling constant with an estimated. error of $\pm 2 \times 10^{-4}$ cm^{-1}.

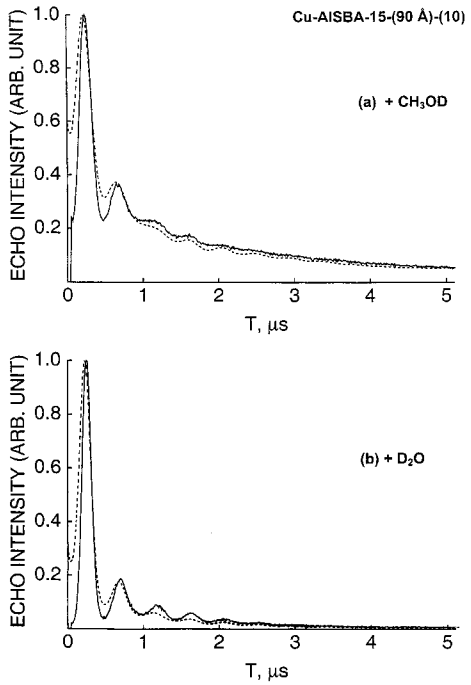

Figure 10. Experimental (—) and simulated (- - -) three pulse ESEM spectra recorded at 4.5 K of dehydrated Cu−AlSBA-15-(90 Å)-(10) with adsorbed (a) CH_3OD and (b) D_2O.

diameter and wall thickness. The pore size measured from N_2 adsorption isotherms is 90 Å (see Figure 2). Thus the wall thickness is 30 Å for SBA-15-(90 Å). This is of the same order as reported for SBA-15 materials by Zhao et al.[5] (38 Å), Luan et al.[10] (43 Å) and Kruck et al.[20] (27 Å). It has been shown in the literature for hexagonal mesoporous materials (MCM-41,[23−25] SBA-15[20]) that the relative intensity of the 200 reflection with respect to the 110 reflection is related to wall thickness. Kruck et al.[20] claimed that samples with more intense 200 reflections compared to 110 reflections have thicker pore walls. In the present case the 200 reflection is relatively less intense compared to the 110 reflection, which is consistent with a smaller wall thickness.

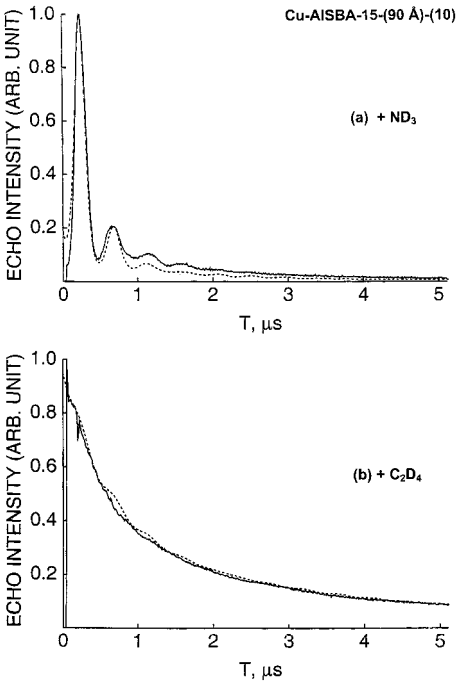

Figure 11. Experimental (—) and simulated (- - -) three pulse ESEM spectra recorded at 4.5 K of dehydrated Cu−AlSBA-15-(90 Å)-(10) with adsorbed (a) ND_3 and (b) C_2D_4.

TABLE 4: ESEM Parameters of Cu−AlSBA-15−(*D* Å)-(Si/Al) Samples with Different Adsorbates

adsorbate	shell	N[a]	R[b] (Å)	A[c] (MHz)
		Cu−AlSBA-15-(90 Å)-(10)		
CH_3OD	1	3	2.8	0.27
D_2O	2	6	2.9	0.29
		6	3.9	0.05
ND_3	1	12	3.1	0.20
C_2D_4	1	4	4.6	0.18
		Cu−AlSBA-15-(170 Å)-(10)		
CH_3OD	1	4	2.8	0.25
D_2O	2	6	3.0	0.20
		6	4.0	0.05
ND_3	1	12	3.3	0.15
C_2D_4	1	4	5.8	0.05
		Cu−AlSBA-15-(230 Å)-(10)		
CH_3OD	1	2	2.8	0.20
D_2O	2	6	3.2	0.10
		6	4.2	0.05
ND_3	1	12	3.2	0.20
C_2D_4	1	4	5.5	0.05

[a] Number of ^{2}D nuclei. [b] Cu(II)-^{2}D distance. [c] Isotropic hyperfine coupling of ^{2}D.

Also, with alumination the XRD peaks shift slightly toward higher 2θ. This can be due either to contraction of the pores or to thinner pore walls. N_2 adsorption isotherms of the AlSBA-15-(90 Å)-(10) show no change in the pore diameter. Hence the shift in the XRD peaks with alumination can be understood as due to thinner pore walls. Also, based on NMR studies, Luan et al.[10] identified aluminum in both tetrahedral framework sites as well as in nonframework octahedral sites. In general, nonframework aluminum will cause the pore size to decrease. Since no such decrease in pore size with alumination is observed, the presence of nonframework aluminum in these samples seems minimal.

ESR and ESEM Studies. ESR and ESEM spectroscopies are powerful tools to determine the location of paramagnetic

transition metal ions in zeolites.[26] The locations of cupric ion in other microporous and mesoporous materials has also been achieved by using these ESEM techniques.[27−31] The spin Hamiltonian parameters of cupric ions are very sensitive to the surrounding ligands and to its site symmetry. For instance, cupric ions with tetrahedral symmetry have spin Hamiltonian parameters in the range of $g_{||} = 2.516$ and $A_{||} = 0.007$ cm^{-1} while with square planar symmetry the parameters are in the range of $g_{||} = 2.245$ and $A_{||} = 0.017$ cm^{-1}. Spin Hamiltonian parameters for cupric ion with distorted octahedral and square pyramidal symmetry are between these values.[32,33] Moreover, if nitrogen is coordinated to Cu(II) ions with a given symmetry, the $A_{||}$ value increases and the $g_{||}$ value decreases as compared to the cupric ions coordinated by oxygens with the same symmetry. For example, the parameters $g_{||} = 2.24$ and $A_{||} = 0.017$ cm^{-1} for nitrogen coordinated to Cu(II) ions indicate an octahedral complex instead of a square planar one.[34] ESEM complements ESR and allows determination of the number of adsorbed molecules together with their distance from the Cu(II) ions. By comparing these data and the spin Hamiltonian parameters with those of known Cu(II) locations in zeolites, it is possible to provide information about the coordination and location of Cu(II) ions in these SBA-15 materials.

In the present work, six different cupric ion species are observed in Cu−AlSBA-15-(90 Å)-(10). A fresh hydrated sample at room temperature shows species A and A′. Species A, with g and A parameters $g_{||}^{A} = 2.369$, $g_{||}^{A} = 2.078$, $A_{||}^{A} = 131 \times 10^{-4}$ cm^{-1}, and $A_{\perp}^{A}$ unresolved, has axial symmetry and indicates Cu(II) ions in a distorted octahedral site. The isotropic signal at $g_{iso}^{A'} = 2.154$ is not the average of $g_{||}^{A}$ and $g_{\perp}^{A}$ (i.e., $[g_{||}^{A} + 2g_{\perp}^{A}]/3$) and hence it can be assigned to Cu(II) ions coordinated with a different number of water molecules than that of species A. Upon cooling to 77 K, the isotropic g line disappears, resulting in a purely anisotropic g, and this species is termed species B. Room-temperature evacuation of this sample for 2 h results in species C, and species D results when the sample is evacuated for 4 h at room temperature. The $g_{||}$ value decreases and the $A_{||}$ value increases upon evacuation. Also, the intensity of isotropic signal A′ decreases after 2 h of evacuation at room temperature and completely disappears after evacuation for 4 h. This may be explained as due to the loss of loosely bound water molecules during evacuation.

Evacuation of the sample at 100 °C for 2 h results in an ESR spectrum with parameters similar to species C, while a new species E results after evacuation for 10 h at 400 °C. After subsequent oxygen adsorption, the cupric ions result in an ESR spectrum similar to that of species D. This means that the cupric ions are in a site that is accessible to oxygen and other adsorbates.

Adsorption of methanol on Cu−AlSBA-15-(D Å)-(10) (D = 90, 170, and 230 Å) results in an axial g spectrum with the parameters listed in Table 3. The spin Hamiltonian parameters of these methanol-adsorbed samples are comparable to those of freshly hydrated samples. Furthermore, the $g_{||}$ value (≈2.373) indicates either a distorted octahedral or square pyramidal coordination of Cu(II) ions with oxygen ligands. ESEM results show that three methanol molecules interact with Cu(II) ions with a Cu(II)−^{2}D distance of 0.28 nm in SBA-15 materials with a 90 Å pore diameter, while four methanol molecules interact with Cu(II) at a distance of 0.28 nm in SBA-15 materials with a pore diameter of 170 Å. Comparing the adsorption of CH_3OD and CD_3OH in AlMCM-41 materials, Pöppl et al.[13] showed that cupric ions complex with CH_3OH through the hydroxyl oxygen. Our ESR and ESEM results are similar to that work,[13] and hence it is reasonable to assume that the Cu(II) ions interact with methanol through the hydroxyl oxygen. Hence for Cu−AlSBA-15-(90 Å)-(10), cupric ions coordinate with three oxygens from methanol molecules and three or two oxygens from the framework. Cu−AlSBA-15-(170 Å)-(10) coordinates with four oxygens from methanol molecules and two or one oxygen from the framework.

Adsorption of D_2O results in an ESR spectrum with parameters similar to those of methanol adsorption. The ESR parameters indicate that distorted octahedral or square pyramidal coordinations are most likely for D_2O in SBA-15 materials. From the ESEM parameters, the cupric ions interact with twelve deuteriums or six water ligands at different distances, as shown in Table 4. This confirms distorted octahedral coordination for cupric ions as $[Cu(H_2O)_6]^{2+}$. Similar hexaaquo coordination of cupric ions has been reported in MCM-41 mesoporous materials.[15,22,28,31]

Cu−AlSBA-15-(90 Å)-(10) with adsorbed NH_3 shows another Cu(II) species with $g_{||} = 2.239$ and $A_{||} = 187 \times 10^{-4}$ cm^{-1}. The $g_{||}$ value decreases and the $A_{||}$ value increases as compared to Cu(II) species A. With adsorbed $^{15}NH_3$ a quintet superhyperfine structure with $A^{N} = 19 \times 10^{-4}$ cm^{-1} is seen, which indicates interaction with four ^{15}N nuclei ($I = {}^1/_2$). The expected intensity ratio of 1:4:6:4:1 is not clear since the intensities overlap the perpendicular g component. However, the spin Hamiltonian parameters are comparable to other tetracoordinated ammonia complexes of Cu(II) ions in Y zeolite[35] ($g_{||} = 2.228$, $A_{||} = 178 \times 10^{-4}$ cm^{-1}) and ρ zeolite[36] ($g_{||} = 2.239$, $A_{||} = 175 \times 10^{-4}$ cm^{-1}) with square planar geometry. Moreover, ESEM studies of samples with adsorbed ND_3 suggest the coordination of four ammonia molecules with the cupric ions. Hence a square planar symmetry is assigned to the cupric ions as a $[Cu-(NH_3)_4]^{2+}$ complex.

After adsorption of ethylene, Cu−AlSBA-15-(D Å)-(10) (D = 90, 170, and 230 Å) materials show ESR spectra somewhat different from their dehydrated samples, indicating some interaction of Cu(II) with ehtylene. However, the ESEM data show that the ethylene−Cu(II) interaction is quite weak because the distance is large. A weak interaction between Cu(II) ions and ^{2}D nuclei at a distance greater than direct coordination with ethylene has also been reported for AlMCM-41.[30]

Conclusions

AlSBA-15 materials with good crystallinity have been synthesized with different pore sizes and ion-exchanged with Cu(II). The room-temperature ESR spectra show two Cu(II) species with axial and isotropic g tensors. The isotropic signal disappears upon cooling to 77 K. The ESR spectra of Cu−AlSBA-15-(90 Å)-(10) show different Cu(II) species upon evacuation due to loss of water molecules. A new Cu(II) species evolves after evacuation at 400 °C for 10 h, and the effect of subsequent addition of oxygen indicates that the Cu(II) ions are accessible to oxygen and to other adsorbates. No significant change in the spin Hamiltonian parameters is observed with the Si/Al ratio but the concentration of cupric ions increases with a decrease in the Si/Al ratio due to greater ion-exchange capacity. Samples with adsorbed methanol or D_2O form a cupric species with octahedral or square pyramidal geometry. After ammonia adsorption a square planar $[Cu-(NH_3)_4]^{2+}$ complex is formed. Ethylene has a much weaker interaction with Cu(II) ions than the above adsorbates and does not show direct coordination with Cu(II). No significant trend in the spin Hamiltonian parameters with different pore sizes is found.

Acknowledgment. This research was supported by the Robert A. Welch Foundation, the Environmental Institute of Houston, and the National Science Foundation. This work made use of a Scintag XDS 2000 automated diffractometer in a MRSEC shared facility supported by the National Science Foundation under Award Number DMR-9632667.

References and Notes

(1) Chon, H., Ihm, S. K., Uh, Y. S., Eds. *Progress In Zeolite and Microporous Materials*; Studies in Surface Science and Catalysis, Vol. 105; Elsevier: Amsterdam, 1997.

(2) (a) Kresge, C. T.; Leonowicz, M. E.; Roth W. J.; Vartuli, J. C.; Back, J. S. *Nature* **1992**, 359, 710. (b) Back, J. S.; Vartuli, J. C.; Roth, W. J.; Leonowicz, M. E.; Kresge, C. T.; Schmitt, K. D.; Chu, C. T.-W.; Olson, D. H.; Sheppard, E. W.; McCullen, S. B.; Higgins, J. B.; Schlenker, J. L. *J. Am. Chem. Soc.* **1992**, *114*, 10834.

(3) (a) Tanev, P. T.; Pinnavaia, T. J. *Science* **1995**, *267*, 865. (b) Bagshaw, S. A.; Prouzet, E.; Pinnavaia, T. J. *Science* **1995**, *269*, 1242.

(4) Zhao, D.; Feng, J.; Huo, Q.; Melosh, N.; Fredrickron, G. H.; Chmelka, B. F.; Stucky, G. D. *Science* **1998**, *279*, 548.

(5) Zhao, D.; Huo, Q.; Feng, J.; Chmelka, B. F.; Stucky, G. D. *J. Am. Chem. Soc.* **1998**, *120*, 6024.

(6) Yang, P.; Wirnsberger, G.; Huang, H. C.; Cordero, S. R.; McGehee, M. D.; Scott, B.; Deng, T.; Whitesides, G. M.; Chmelka, B. F.; Buratto, S. K.; Stucky, G. D. *Science* **2000**, *287*, 465.

(7) Yang, P.; Zhao, D.; Chmelka, B. F.; Stucky, G. D. *Chem. Mater.* **1998**, *10*, 2033.

(8) Winkel, P. S.-; Lukeni, W. W.; Zhao, D.; Yang, P.; Chmelka, B. F.; Stucky, G. D. *J. Am. Chem. Soc.* **1999**, *121*, 254.

(9) Han, Y.-J.; Stucky, G. D.; Butler, A. *J. Am. Chem. Soc.* **1999**, *121*, 9897.

(10) Luan, Z.; Hartmann, M.; Zhao, D.; Zhou, W.; Kevan, L. *Chem. Mater.* **1999**, *11*, 1621.

(11) Yue, Y.; Gedeon, A.; Bonardet, J.-L.; Melosh, N.; D'Espinose, J.-B.; Fraissard, J. *Chem. Commun.* **1999**, 1967.

(12) Kevan, L.; Hartmann, M. In *Electron Paramagnetic Resonance*; Gilbert, B. C., Atherton, N. M., Davier, M. J., Eds.; Royal Society of Chemistry: Cambridge, U.K., 1998; Vol. 16, pp 199−210.

(13) Pöppl, A.; Hartmann, M.; Kevan, L. *J. Phys. Chem.* **1995**, *99*, 17251.

(14) Prakash, A. M.; Kevan, L. *Langmuir* **1997**, *13*, 5341.

(15) Yu, J.-S.; Kim, J. Y.; Kevan, L. *Micropor. Mesopor. Mater.* **2000**, *40*, 135.

(16) Barrett, E. P.; Joyner, L. G.; Halenda, P. P. *J. Am. Chem. Soc.* **1951**, *73*, 373.

(17) Kevan, L. In *Modern Pulsed and Continuous-Wave Electron Spin Resonance*; Kevan, L., Bowman, M. K., Eds.; Wiley: New York, 1990; pp 231−266.

(18) Kevan, L. In *Time Domain Electron Spin Resonance*; Kevan, L., Schwartz, R. N., Eds.; Wiley: New York, 1979; pp 279−342.

(19) An increase in 2θ values of reflection (say from 100 or 200 planes) indicates a decrease in lattice spacing (d_{100} or d_{200}), which in turn indicates a decrease in the lattice unit cell parameter. The lattice unit cell parameter is the sum of the pore diameter and the wall thickness. Hence a change in the unit cell parameter reflects a change in either or both the pore diameter and wall thickness.

(20) Kruck, M.; Jaroniec, M.; Ko, C. H.; Ryoo, R. *Chem. Mater.* **2000**, *12*, 1961.

(21) Sing, K. S. W.; Everett, D. H.; Haul, R. A. W.; Moscow, L.; Pierotti, R. A.; Rouquerol, J.; Siemieniewska, T. *Pure Appl. Chem.* **1985**, *57*, 603.

(22) Pöppl, A.; Kevan, L. *Langmuir* **1995**, *11*, 4486.

(23) Feuston, B. P.; Higgins, J. B. *J. Phys. Chem.* **1994**, *98*, 4459.

(24) Kruck, M.; Jaroniec, M.; Sayari, A. *Chem. Mater.* **1999**, *11*, 492.

(25) Årgen, P.; Lindén, M.; Rosenholm, J. B.; Schwarzenbacher, R.; Kriechbaum, M.; Amenitsch, H.; Laggner, P.; Blanchand, J.; Schüth, F. *J. Phys. Chem. B* **1999**, *103*, 5943.

(26) Kevan, L. *Acc. Chem. Res.* **1987**, *20*, 1.

(27) Chen, X.; Kevan, L. *J. Am. Chem. Soc.* **1991**, *113*, 2861.

(28) Pöppl, A.; Newhouse, M.; Kevan, L. *J. Phys. Chem.* **1995**, *99*, 10019.

(29) Wasowicz, T.; Prakash, A. M.; Kevan, L. *Micropor, Mater.* **1997**, *12*, 107.

(30) Kim, J. Y.; Yu, J.-S.; Kevan, L. *Mol. Phys.* **1998**, *95*, 989.

(31) Xu, J.; Yu, J.-S.; Seung, J. L.; Kim, B. Y.; Kevan, L. *J. Phys. Chem. B* **2000**, *104*, 1307.

(32) Tominaga, H.; Ono, Y.; Keii, T. *J. Catal.* **1975**, *40*, 197.

(33) Hathaway, B. J.; Billing, D. E. *Coord. Chem. Rev.* **1970**, *5*, 143.

(34) Hathaway, B. J.; Tomlinson, A. A. G. *Coord. Chem. Rev.* **1970**, *5*, 1.

(35) Vansant, E. F.; Lunsford, J. H. *J. Phys. Chem.* **1972**, *76*, 2860.

(36) Anderson, M. W.; Kevan, L. *J. Phys. Chem.* **1987**, *91*, 2926.